Journal of Metals, Materials and Minerals, Vol. 31, No. 3, pp. 143-151, 2021

Characteristic of fluorescence spectroscopy response of tetrakis (4-sulfonatophenyl) porphyrin doped polyaniline toward Fe^{3+} ion

Chatr Panithipongwut KOWALSKI[1,*], Meatawadee BUNTEE[2], and Prasit PATTANANUWAT[1,*]

[1] *Department of Materials Science, Faculty of Science, Chulalongkorn University, Bangkok, 10330, Thailand*
[2] *Petrochemistry and Polymer Science, Faculty of Science, Chulalongkorn University, Bangkok, 10330, Thailand*

***Corresponding author e-mail:** chatr.p@chula.ac.th, prasit.pat@chula.ac.th

Received date:
16 July 2021
Revised date
21 August 2021
Accepted date:
24 August 2021

Keywords:
Polyaniline;
Tetrakis (4-sulfonatophenyl) porphyrin;
Fluorescence sensing;
Fe^{3+} detection

Abstract

Here, we report a selective colorimetric chemosensor toward Fe^{3+} ion detection by the combination of sensitizer and hole transport consisting of polyaniline and tetrakis (4-sulfonatophenyl) porphyrin. Interestingly, the presence of tetrakis (4-sulfonatophenyl) porphyrin moiety on polyaniline can enhance the optical limiting properties of polyaniline, allowing the fluorophore signal for chemical sensor. The performance sensing behaviors toward metal ion are observed by the ultraviolet-Visible and fluorescence properties. The sensing of polyaniline-tetrakis (4-sulfonatophenyl) porphyrin toward Fe^{3+} ion exhibits a linear response in the concentration range of 0.01 M to 1.0×10^{-4} M over the other transition metals (Cu^{2+}, Ni^{2+}, Zn^{2+}, Pb^{2+}, Cd^{2+}, Mn^{2+}, B^{2+} and Ag^{+}). A turn-off color of fluorescence emission can be applied for the rapid visualization of Fe^{3+} ion. The effective response of pH-independent Fe^{3+} ion sensing of polyaniline-tetrakis (4-sulfonatophenyl) porphyrin by quenching fluorescence reveals sufficiency in range of 4.0-12.0.

1. Introduction

Iron is one of the dangerous heavy metals and globally widespread pollutants in environment. The iron in the human body needs to regulate the level because it is an essential element in hemoglobin and plays major role for the transportation of oxygen to tissues. However, high concentrations of iron can cause serious health problem. The iron ion possesses the high potential of biological toxicity, and thereby leads to cause effect on living organisms including fatigue, immunity, and hemochromatosis. The cause of cellular toxicity of iron ions level in human body can initiate the serious diseases such Alzheimer's, Huntington's and Parkinson's disease [1]. Chronic inhalation of excessive concentrations of iron oxide fumes may cause an evolution of pneumoconiosis. Thus, monitoring and detection of iron ions are in emerging demand.

Recently, the detection techniques for transition metal ion levels have been developed including atomic absorption spectrometry (AAS) [2], inductively coupled plasma-atomic emission spectrometry (ICP-AES) [3], and voltammetry [4]. Among them, a simple technique for achieving detection, the optical sensor based on UV-Visible and fluorescence spectrophotometer have been developed for the relatively less expensive instruments and the cheap sample preparation. Principally, UV-Vis and fluorescence spectrophotometer demonstrates the analysis on multi-ions without expensive sample. These operations focus on exploring the different organic structures with optical properties to determine the targeted metal ions, which can be easily observed with the naked eye. Furthermore, fluorescent chemosensor has been designed for architectural and material techniques because of their chemical structure such as unique, tunable, sensitivity and selectivity [5,6]. More attention has been studied in fluorescence materials for transition metal ion detection, which is principally based on small molecules. In the recent years, the research works on conjugated polymer-based fluorescence sensors in current interest area for specific target anions or cations have gained increase attention due to their high sensitivity [5-8]. The electron energy migration passes along the conjugated backbone upon excitation, thereby resulting in amplifying the signal with high sensitivity for target metal ion detection. Among the conjugated polymers, PANi is a good candidate to study the electronic and optical applications because the unique property of PANi have been widely studied in chemosensor with functionalization by different dopants. Its structure can be utilized in electron transfer process, serving as either electron acceptor or electron donor which is depended on the relative positions of redox potential of dopant molecule and PANi [9-11].

Porphyrin moiety has been widely employed as a good signal moiety of a fluorescence sensor due to their advantageous photo-physical characteristics. The wide varieties of porphyrin-based structure with their modulating functionality are of fascinating fields of chemistry, biological technology, materials science, photosensitizers, catalysis, and sensor applications. The aggregate supramolecules of well-defined porphyrin relies on non-covalent interactions (electrostatic, hydrogen bond, π-π, or coordinative interaction). This characteristic porphyrin attributes the achievement of recognition properties with different chiroptical and molecular [12-14].

In this research work, the incorporation of polyaniline (PANi) with porphyrin, namely tetrakis (4-sulfonatophenyl) porphyrin (TPPS), is firstly proposed to obtain the extraordinary properties toward its electronic and optical properties. To our knowledge, the development

of PANi-TPPS sensing toward the electronic and optical properties for chemosensor has not widely studied. Furthermore, the report of a novel of fluorescent chemosensor based on the conjugated polymer of TPPS doped PANi for Fe^{3+} detection in comparison to other cations, such as Cu^{2+}, Ni^{2+}, Zn^{2+}, Pb^{2+}, Cd^{2+}, Mn^{2+}, B^{2+} and Ag^{+} is examined.

2. Experimental

2.1 Chemical

Pyrrole (99% purity, Tokyo Chemical Industry) and aniline (99% purity, Tokyo Chemical Industry) were distilled under a reduced pressure and stored in the dark before being used. Benzaldehyde (99% purity, Tokyo Chemical Industry), Ammonium persulfate (95% purity, nacalai tesque), sodium hydroxide (97% purity, chameleon) and sulfuric acid (95% to 98% purity, nacalai tesque) were of analytical grade and used without further purification. Dimethyl sulfoxide (99% purity, Tokyo Chemical Industry) was distilled and used as a solvent. Water was distilled before use. All other chemicals were analytical grade and were used as received.

2.2 Synthesis of tetraphenylporphyrin (TPP) and tetrakis (4-sulfonatophenyl) porphyrin (TPPS)

The synthesis method of TPPS was ascribed earlier [15], for TPP synthesis, 1 L of propionic acid was typically refluxed in two-necked round bottomed flask and followed by gradual adding 0.8 M pyrrole and 0.8 M benzaldehyde during the period of 10 min, respectively. The mixture reaction was further refluxed for 1 h, cooled down at room temperature and precipitated in methanol overnight. TPP product was filtered and washed with methanol several time to remove the unreacted TPP. TPPS was synthesized by sulfonation of 0.5 g TPP with 50 mL concentrated sulfuric acid at 100°C to 110°C. The mixture product was isolated by precipitating in acetone, followed by centrifugation at 8000 rpm for 10 min and filtered through G-4 sintered glass crucible. The sulfuric acid and unreacted TPP was removed with acetone several times. The obtained green products (protonated form of TPPS) were dried in oven at 50°C.

2.3 Polymerization of tetrakis (4-sulfonatophenyl) porphyrin-doped polyaniline (PANi-TPPS)

In this experiment, PANi containing TPPS dopant was synthesized following the synthesis method establishes earlier [16,17]. Firstly, 0.1 g of TPPS was neutralized by using dilute aqueous NaOH solution at 0°C to 2°C. Then, 0.5 mL aniline monomer was added into the above mixture solution (stoichiometric aniline: sodium salt of TPPS ratio at 1:0.0015). Subsequently, 1.44 g of ammonium persulfate (APS) was dissolved in water at 2°C and then was slowly dropped during the period of 10 min. The pH mixture solution was changed to 5 after APS adding. The polymerization was continuously stirred and carried out at 0°C to 2°C for 8 h. The green product was filtered, washed with water and acetone until the filtrated solution is colorless. The final green product was dried in oven at 50°C overnight.

2.4 Optical absorption and fluorescence spectroscopy

The functional groups of PANi and PANi-TPPS were examined by Fourier transform infrared spectroscopy (FT-IR: Nicolet 6700, Thermo scientific). UV-Visible spectra were performed on a Shimadzu UV-315 (Jasco model 7800) at room temperature. Fluorescence excitation, emission spectra and quantum yield were measured on an Edinburgh-FLS 920 Combined Fluorescence Lifetime and Steady State Spectrometer at room temperature with the slit width of 1 nm. Quartz cuvettes with a 3 cm path length used for all fluorescence measurements. For a typical experiment, the aliquots of a Fe^{3+} (0.01 M to 1.0×10^{-4} M in 0.275 M HNO_3) or other metal ion were added to a 3 mL solution of PANi-TPPS (0.067 mg·ml^{-1} in DMSO) by a syringe. The metal ion dependent fluorescence intensity was obtained by monitoring the emission intensity at 648 nm with repeated 10 times. For all experiments, the excitation wavelengths were fixed at 421 nm.

3. Results and discussion

The synthetic procedure of the polyaniline doped tetrakis (4-sulfonatophenyl) porphyrin synthesis is demonstrated as shown in Figure 1. Figure 2 presents the FT-IR spectrum of the as synthesized TPPS dopant on PANi and TPPS. It is obviously seen that PANi-TPPS spectrum demonstrates the main peaks at 1328, 1242, 1024, and 870 cm^{-1} which are corresponded to C-H stretching vibration, C-N stretching vibration in benzenoid ring, C=C bending vibration of quinoid ring and C-H out of plane deformation vibrations for aromatic ring, respectively. The observed peak at 979 cm^{-1} and 1244 cm^{-1} are assigned to the S=O stretching of sulfonate and sulfoxide from TPPS on PANi, respectively, suggesting the successful TPSS doping on PANi [15,16]. Electronic absorption spectra of TPPS and PANi-TPPS in DMSO solution are showed in Figure 3(a). It is seen that the absorbance spectrum of TPPS exhibits a sharp and intense peak of Soret band at 421 nm, following by several weaker absorptions (Q bands) at higher wavelengths (from 450 nm to 700 nm). In contrast, UV-Vis spectrum of PANi-TPPS exhibits all the spectrum characteristics band of TPPS with the extra absorbance spectrum at 350 nm. This characteristic band at 325 nm is attributed to π-π* transition of conjugate system in PANi salt. These optical absorption characteristics confirm the presence of TPPS on PANi molecule [12].

Figure 3(b) exhibits the typical fluorescence spectrum of PANi-TPSS in DMSO at the λ emission of 420 nm. The spectrum reveals a strong band at 647 nm, followed by the shoulder band at 710 nm. The presence of the two emission bands is evidence support for the formation of tetraanion of TPPS as PANi-TPPS salt in the structure. All results from FT-IR, UV-Vis, and fluorescence spectra of PANi-TPPS are in good agreement with the earlier reports [15-17].

3.1 Effect of pH on UV-Vis and fluorescence sensing of PANi-TPPS

The characteristic pH-dependent absorption spectrum of PANi-TPPS is showed as seen in Figure 4(a). Obviously, the absorption spectra of Soret-band and Q-band of TPPS plays a key role in the changing of excitonic absorption band at different pH. As mentioned

before, the absorbance spectrum of TPPS at the neutral pH shows the Soret band at 421 nm, following by several weaker Q bands. At very low pH (≤ 3), the appearance of the red shift at 447 nm (J-band) due to the formation of the J-aggregates in aqueous solutions is observed. The TPPS dopant in PANi is protonated spontaneously to form the coordination complex of H^+ with nitrogen atom in pyridine of macrocyclic-ring (H_4TPPS^{2-}), thereby leading to completely split the π-electron conjugated system of TPPS. Up to pH 3, the electronic absorption spectral of PANi-TPPS exhibits the decrement in intensity at 447 nm and the increment in intensity at 421 nm. The excitonic absorption band of the blue shift at 421 nm is observed due to the H-aggregates. The presence of both J- and H-aggregates under such condition is occurred due to the acid-base equilibrium existing between unprotonated tetraanion (H_2TPPS^{4-}) and protonated dianion (H_4TPPS^{2-}). However, at high pH (≥ 6), the Soret band at 421 nm is almost identical upon the increasing pH because the H^+ ion concentration is not efficiency to coordination complex within pyridine-ring of TPPS. The PANi-TPPS should be completely deprotonated from H^+ ion, thereby resulting in having a similar nuclear shielded/ deshielding at tetrapyrrole and tetraphenyl sites. This consequence presented herein is similar to the previous report, the red shift of the Soret band (434 nm versus 412 nm) of TPPS is related to the de-protonation of the macrocyclic nitrogen centers in porphyrin. The pKa for the protonation of macrocyclic ring is about pH ≥ 4.8 which corresponds agreement in this experiment[18,19]. Furthermore, the appearance of the absorbance spectrum of the π-π* transition of the benzenoid ring in PANi at 325 nm reveals the sharp increase in intensity with increasing pH. Principally, the characteristic bands of PANi doped TPPS are observed at 325 nm and 640 nm. The increasing of the acid doping concentration causes these bands to decrease in signal intensity [18,20]. Obviously, the increasing degree of protonation by decreasing the pH results in the change of the band intensity at 325 nm.

Besides the UV spectroscopy, Figure 4(b) shows the ratio-metric fluorescent sensing for the emission spectra of PANi-TPPS solution in DMSO when is added into different buffer solution with pH ranging from 2 to 10. It is seen that the fluorescence of PANi-TPPS at 647 nm is highly quenched by protonation of hydrogen ions. The amount of fluorescence quenching is related to pH condition. When the pH is reduced from 10 to 6, the fluorescence intensity is gradually decreased. Obviously, the florescence intensity is remarkably decreased at pH ≤ 6. The fluorescence quenching upon varying pH considering as the center core of TPPS which is subjected to protonate by H^+ ion, results in splitting of the π-electron conjugated system of TPPS.

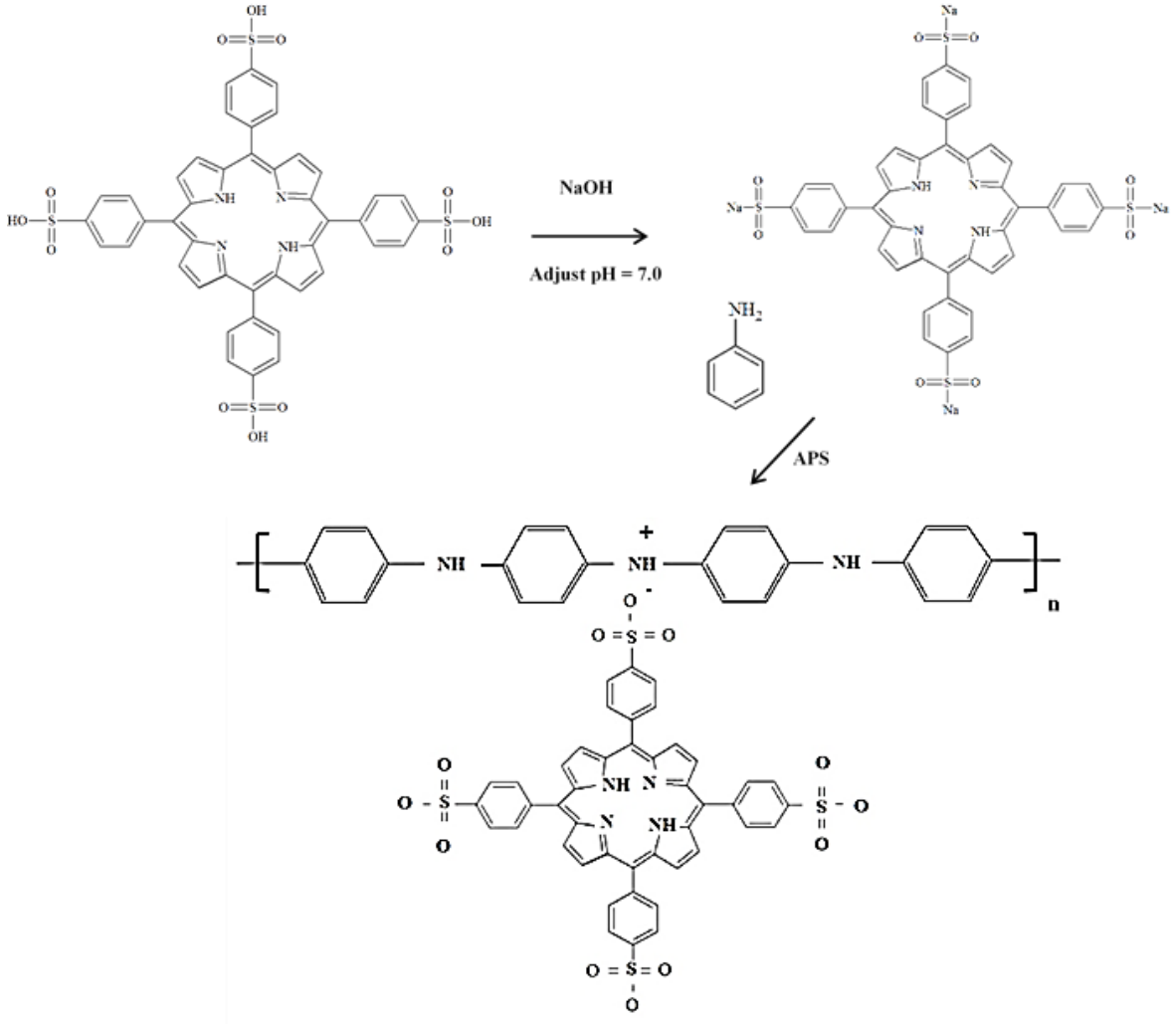

Figure 1. The procedures of the polyaniline doped tetrakis (4-sulfonatophenyl) porphyrin synthesis.

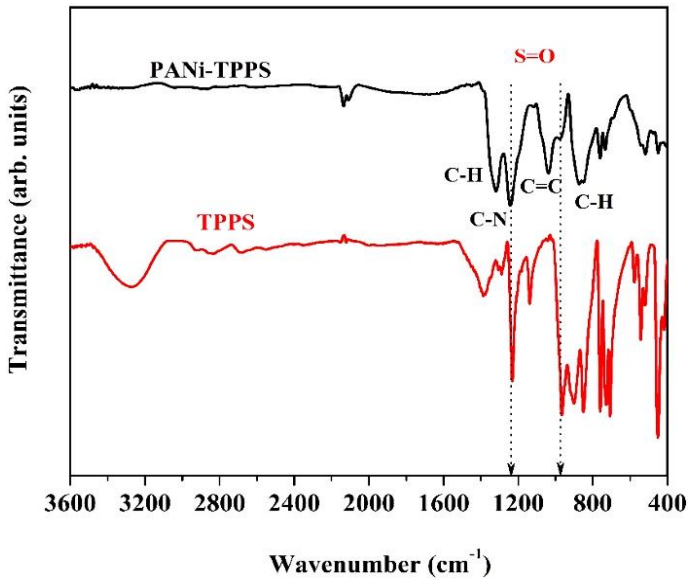

Figure 2. FT-IR spectrum of the TPPS and TPPS doped PANi.

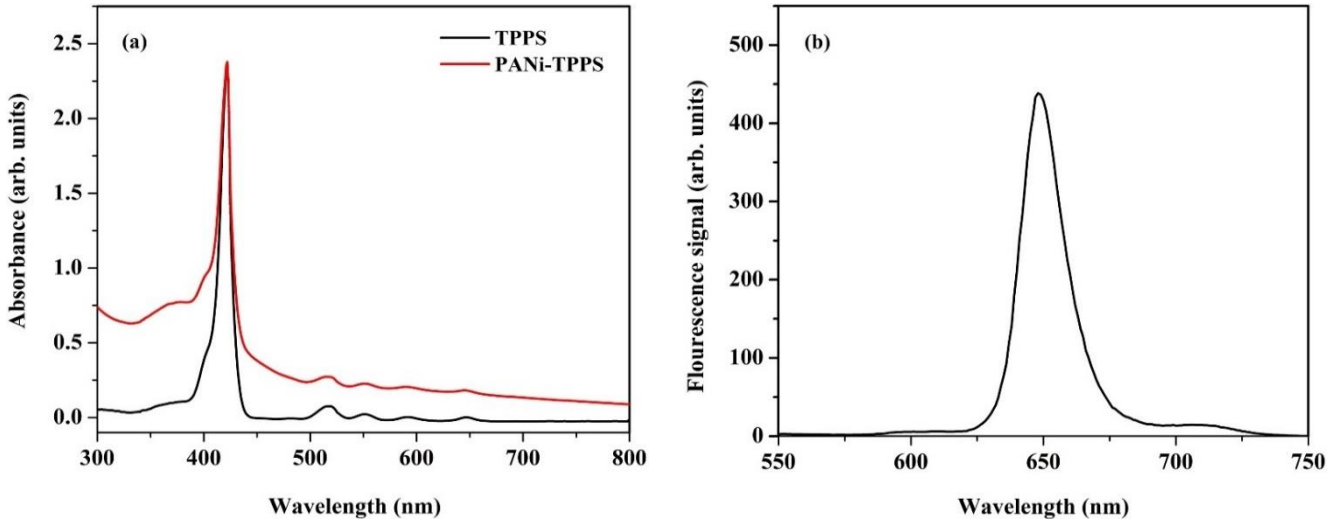

Figure 3. (a) UV-Vis spectrum of the TPPS and PANi-TPPS (b) Fluorescence emission spectrum of TPPS doped PANi.

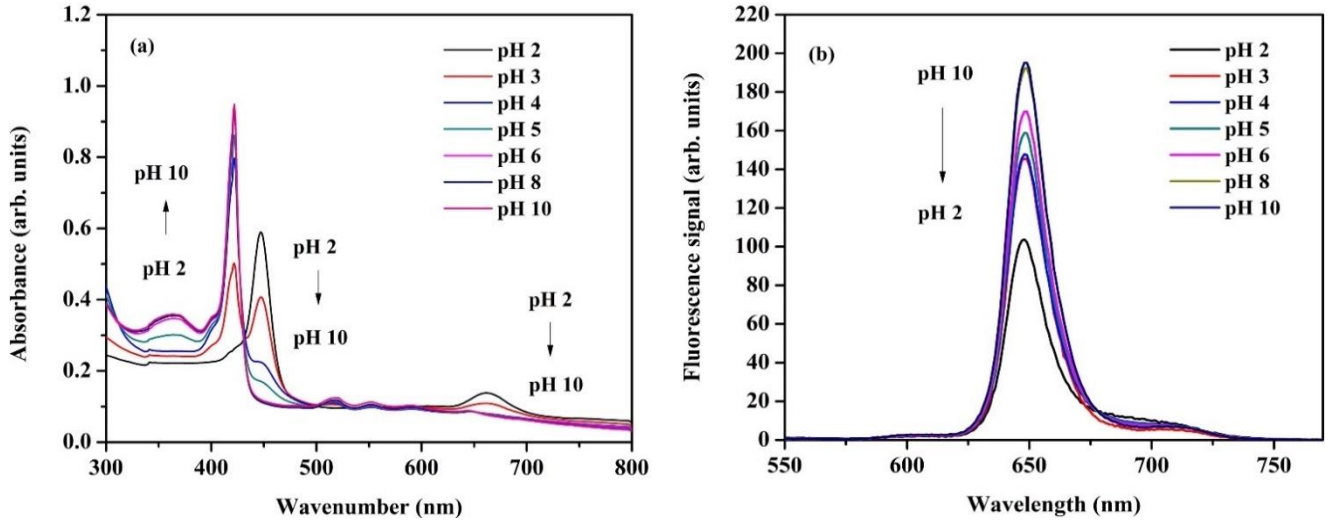

Figure 4. pH sensing spectrum of PANi-TPPS for (a) UV–Vis spectrum and (b) fluorescence spectrum.

3.2 Fluorescence sensing of PANi-TPPS toward metal ion

The fluorescent behaviors of PANi-TPPS towards metal ions are investigated by interactions with the representative alkali (K^+, Li^+, Na^+), alkaline earth (Mg^{2+}, Ca^{2+}), and transition-metal ions (Fe^{3+}, Cu^{2+}, Ni^{2+}, Zn^{2+}, Pb^{2+}, Cd^{2+}, Mn^{2+}, B^{2+}, Ag^+) at concentrations in the range of 0.01 M to 1.0×10^{-4} M. To screen the fluorescent sensor property, the colorimetric responses of PANi-TPPS under fluorescence at λ excited of 421 nm with the different aforementioned metal ions at 1.0×10^{-4} M are examined as shown in Figure 5(a). At 1.0×10^{-4} M of the selected metal ion, the intensity spectrums of PANi-TPPS are remarkably quenched at the wavelength of 647 nm and at 710 nm for Fe^{3+} ion. This result obviously shows the high selectivity and sensitivity of PANi-TPPS against Fe^{3+} relative to the other cations. A colorimetric signal of PANi-TPPS for Fe^{3+} ions presents the discrimination color over the other metal ions under UV-Vis irradiation (Figure 5(b)).

Furthermore, the analysis of relative fluorescence titration is performed to determine the selectivity and sensitivity of PANi- TPPS toward the selected metal ions at concentration of 0.01 M to 1.0×10^{-4} M. The relative intensity response (I_o/I) of PANi-TPPS at band 647 nm with targeted metal ions are calculated as shown in Figure 6. PANi-TPPS exhibits the strong selectivity and sensitivity on Fe^{3+} ion. The relative intensity response (I_o/I) at band 647 nm is remarkably increased with increasing Fe^{3+} concentration. In contrast, the slight increment in the relative intensity response is observed in the presence of Cu^{2+} ion. Meanwhile, the fluorescence quenching responses of the other competitive metal ions could not be easily affected. Similar results are observed for the alkali and alkali earth, which are less efficiency in changing the maximum intensity of the fluorescence.

More importantly, the concerning in Fe^{3+} relative fluorescence sensing by comparison between TPPS and PANi-TPPS behaviors is observed in concentration range of 0.01 M to 1.0×10^{-4} M. As shown in Figure 7(a), the addition of Fe^{3+} to TPPS provides the fluorescence enhancement in intensities at 647 nm and 710 nm by coordinating of TPPS with Fe^{3+}. In contrast, PANi-TPPS reveals oppositely the responses by quenching in the intensities at 647 nm and 710 nm (Figure 7(b)). In fact, the formation of the aggregates of TPPS within PANi-TPPS can enhance the optical limiting property compared to the precursor compounds [15]. Based on this, the insertion Fe^{3+} into TPPS doped PANi may provide inefficient site for energy migration, resulting in the quenching of the fluorescent property. Figure 7c reveals the Stern-Volumer plot of the fluorescence quenching of PANi-TPPS toward Fe^{3+} ion. The linear concentration range of Fe^{3+} detection is calculated between 0.01 M to 0.1×10^{-4} M with the coefficient of determination (R^2) of 0.9896. The limit of detection (LOD) of 0.3972 µM is found for Fe^{3+} (based on a 3σ/slope, where σ is the standard deviation of the blank signal (I_o) without Fe^{3+}). The limit of quantification (LOQ) is 1.324 µM (based on a 10 σ/slope).

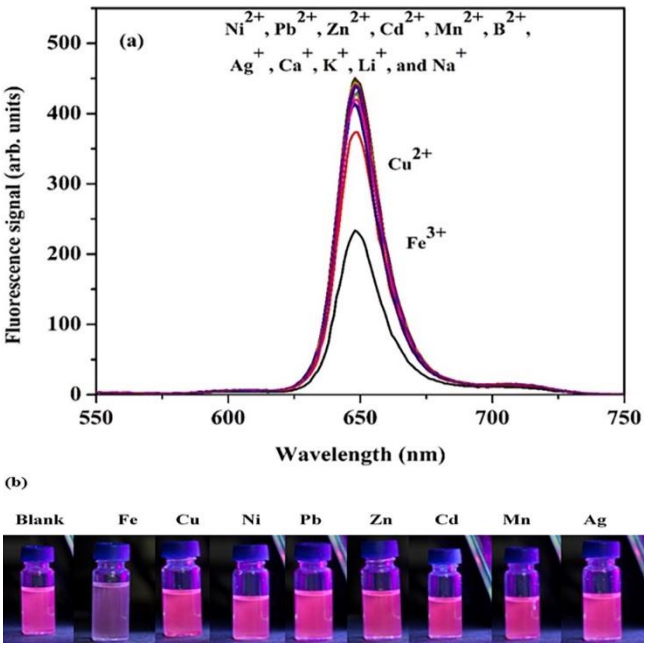

Figure 5 (a) fluorescence response of PANi-TPPS at band 647 nm with different metal ions at 1.0×10^{-4} M (b) Colorimetric response of PANi-TPPS with the addition of various metal ions at $1.0x10^{-4}$ M under UV irradiation.

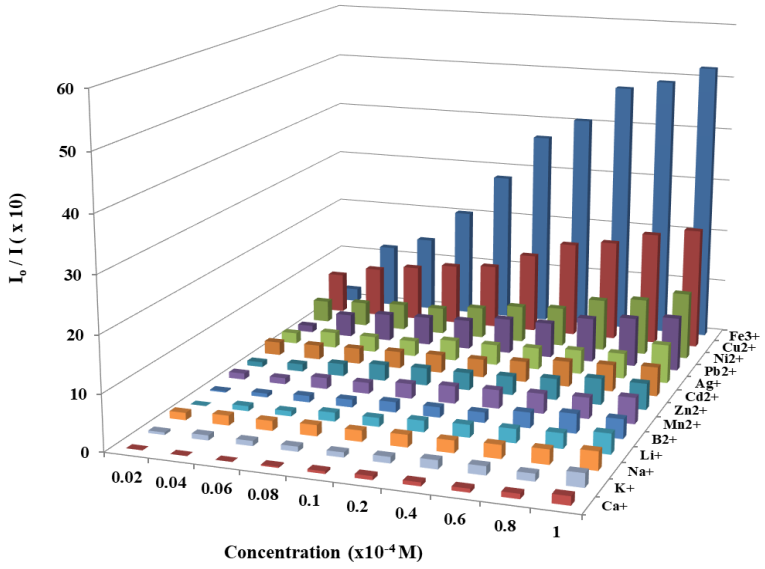

Figure 6. The titration relative intensity of fluorescence response (I_o/I) of PANi-TPPS at band 647 nm with different metal ions at 0.01 M *to* 1.0×10^{-4} M.

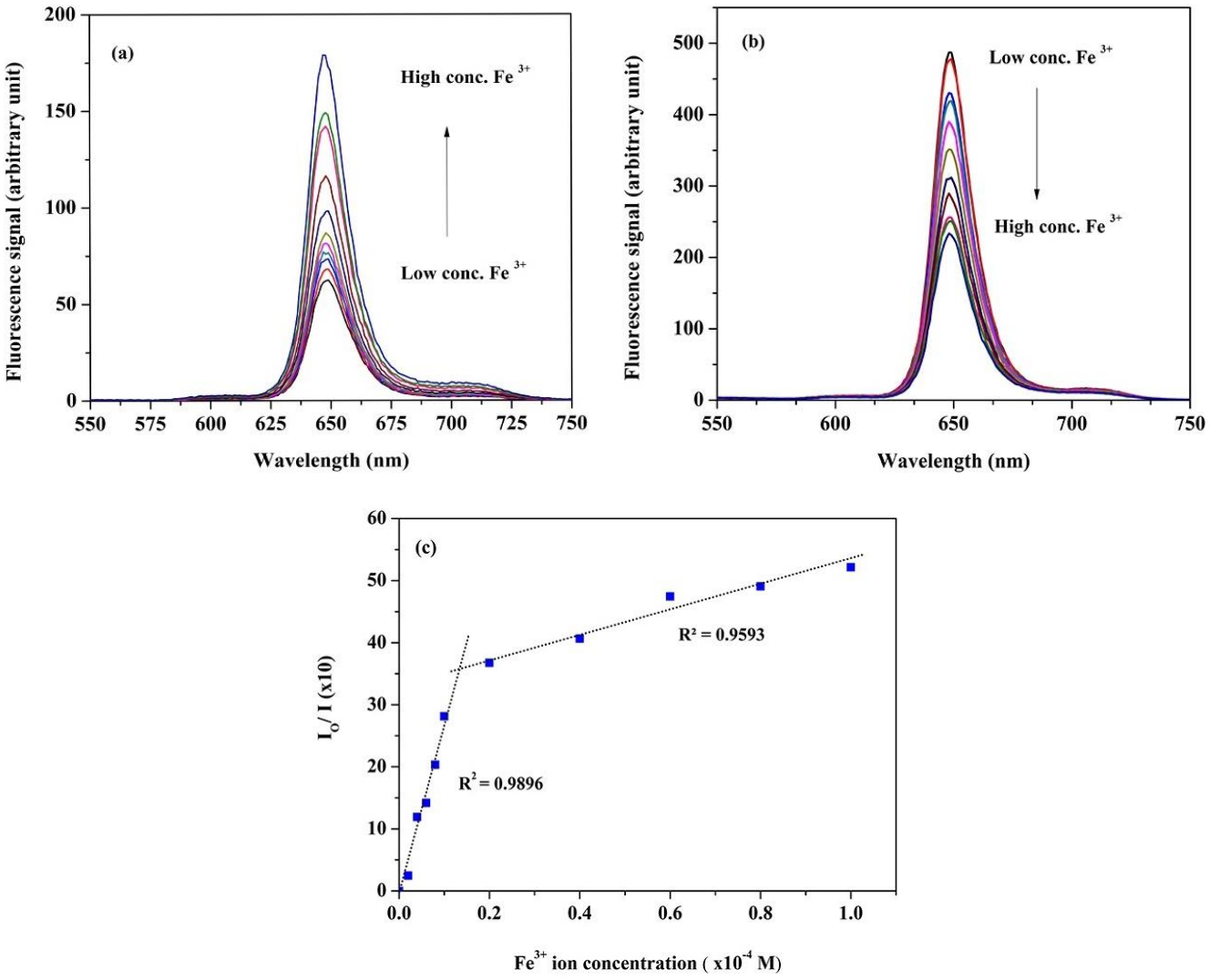

Figure 7. The titration relative intensity of fluorescence response for Fe^{3+} sensing of (a) TPPS (b) PANi-TPPS (excited at λ_{max} 421 nm) (c) Stern-Volumer plot of the fluorescence quenching of PANi-TPPS toward Fe^{3+}.

In addition, the ability of TPPS and PANi-TPPS to recognize Fe^{3+} is further drastically demonstrated by virtue of the electronic absorption titration at 0.01 M to 1.0×10^{-4} M as shown in Figure 8(a) and (b), respectively. As seen in Figure 8(b), the essentially identical absorption bands of the PANi-TPPS in the maximum of the Soret band occurs at 421 nm, while the Q-band region are at 524, 560, 601 and 652 nm, respectively. The additional broad bands beginning at 380 nm are ascribed to the π-π* transitions of the conjugated system in the PANi salt. In the presence of Fe^{3+} ion, the Soret band of PANi-TPPS is significantly affected to decrease and shifted to the red-shift (30 nm) with increasing Fe^{3+} ion. The Q-bands of PANi-TPPS are merged into a new single peak at 675 nm. The intensities of the Soret band gradually decrease, while those of the other new two bands at 453 nm and 675 nm are increased with increasing Fe^{3+} concentration. These spectral changes are characteristics of nitrogen pyridine ring structure in PANi-TPPS. Furthermore, the electronic absorbance of the π-π* transition in the PANi salt beginning at 380 nm is induced with the increasing Fe^{3+} concentration. Comparing to PANi-TPPS, similar results of TPPS UV-Vis spectrum (Figure 8(a)) are observed at 453 nm and 675 nm by increasing in intensity with Fe^{3+} concentration. However, there is a less significant change for the Soret band at 421 nm.

Concerning in the effect of pH on Fe^{3+} sensing of PANi-TPPS, the intensity responses at band 647 nm of PANi-TPPS with and without Fe^{3+} under different the pH conditions are investigated as shown in Figure 9. The plots clearly indicate the interfering effect of protonation at pH ≤ 4 as the presence of the J-and H-aggregates, implying that the effective sensing of PANi-TPPS toward Fe^{3+} is in range of the pH 4.0 to 12.0. The comparison of the present results with those of the other materials for Fe^{3+} detection is listed in Table 1. As can be seen, the limit of detection of PANi-TPSS in this research is lower than most of the other sensing materials. Meanwhile, the wider working range in pH environment is also obtained in this work.

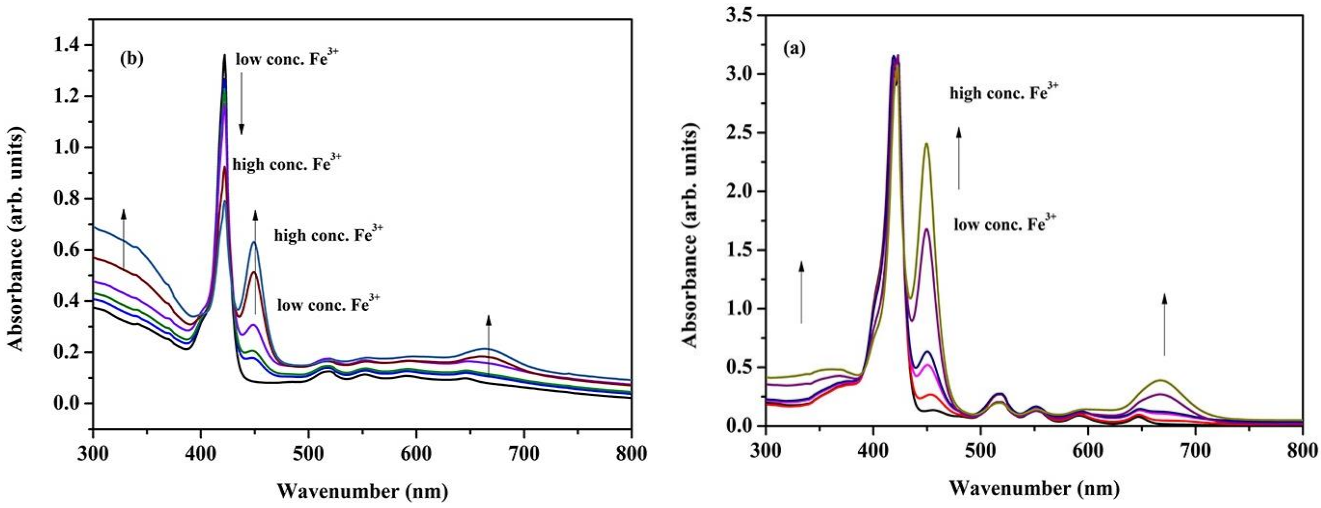

Figure 8. The titration relative intensity of UV-Vis spectrum response for Fe^{3+} sensing of (a) TPPS (b) PANi-TPPS.

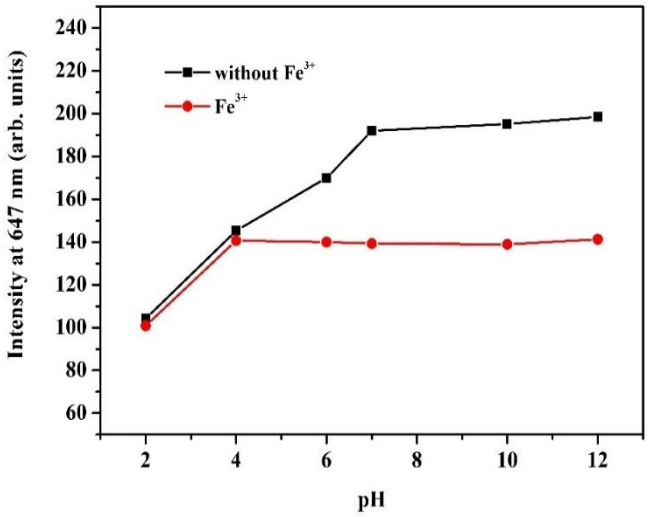

Figure 9. The effect of pH on intensity of fluorescence sensing toward Fe^{3+} detection of PANi-TPPS.

Table 1. The comparative results of the fluorescent material sensing toward Fe^{3+}.

Material Sensing	LOD	pH	Reference
β-cyclodextrins and 2,6-bis(benzoxazolyl)pyridine	0.6 µM	> 3.6	21
1,8-naphthalimide	2.0 µM	4.0-9.0	22
MXene quantum dots	0.31 µM	6.4-8.4	23
Fe_3O_4@ZnO	3.0 nM	4.9-7.3	24
Phosphazene	4.8 µM	at 7.4	25
5-nitroisatin Schiff /SBA-15	1.49 mM	-	26
Ethylenediamintetraacetic acid-nickel-base	1.0 nM	at 4.5	27
Polyepinephrine-based fluorescent organic dots	0.671 µM	at 7.4	28
Pyrene-based Schiff-base	31.9 µM	at 7.4	29
PANi-TPPS	0.39 µM	4.0-12.0	(This work)

4. Conclusions

The synthetic versatility of TPPS dopant onto PANi allows the using of TPPS moiety as the signaling fluorophore, possessing a strong binding affinity as well as a strong sensitivity and selectivity for Fe^{3+} ion. The enhancing of PANi-TPPS material sensing toward Fe^{3+} ion is presented as a quenching of the emission intensity characteristic with the titration ratio of the fluorescence signal. The selectivity of PANi-TPPS toward Fe^{3+} over other metal ions is remarkably high, and its sensitivity is below 0.01×10^{-4} M in aqueous solutions. Conceivable applications also include the use as pH sensors by monitoring the UV-Vis and fluorescence properties. This study opens a new opportunity for designing PANi-based multicolor fluorescent chemosensor in other applications such as electrochromic device, biotechnologies, etc.

References

[1] M. B. H. Youdim, G. Stephenson G, and D. B. Shachar, "Ironing iron out in Parkinson's disease and other neurodegenerative diseases with iron chelators: a lesson from 6-hydroxy-dopamine and iron chelators, desferal and VK-28," *Annals of the New York Academy of Sciences*, vol. 1012 pp. 306-325, 2004.

[2] H. Bağ, M. Lale, and A. R. Türker, "Determination of iron and nickel by flame atomic absorption spectrophotometry after preconcentration on Saccharomyces cereVisiae immobilized sepiolite," *Talanta*, vol. 47, no. 3, pp. 689-696, 1998.

[3] K. S. Rao, T. Balaji, T. P. Rao, Y. Babu, and G. R. K. Naidu, "Determination of iron, cobalt, nickel, manganese, zinc, copper, cadmium and lead in human hair by inductively coupled plasma-atomic emission spectrometry," *Spectrochimica Acta Part B: Atomic Spectroscopy*, vol. 57, no. 8, pp. 1333-1338, 2002.

[4] J. N. Butt, F. A. Armstrong, J. Breton, S. J. George, A. J. Thomson, and E. C. Hatchikian, "Investigation of metal ion uptake reactivities of [3Fe-4S] clusters in proteins: voltammetry of co-adsorbed ferredoxin-aminocyclitol films at graphite electrodes and spectroscopic identification of transformed clusters," *Journal of the American Chemical Society*, vol. 113, no. 17, pp. 6663-6670, 1991.

[5] T. Wang, N. Zhang, W. Bai, and Y. Bao, "Fluorescent chemosensors based on conjugated polymers with N-heterocyclic moieties: two decades of progress," *Polymer Chemistry*, vol. 11, no. 18, pp. 3095-3114, 2020.

[6] D. Wu, A. C. Sedgwick, T. Gunnlaugsson, E. U. Akkaya, J. Yoon, and T. D. James, "Fluorescent chemosensors: the past, present and future," Chemical Society Reviews, vol. 46, no. 23, pp. 7105-7123, 2017.

[7] L. Basabe-Desmonts, D. N. Reinhoudt, and M. Crego-Calama, "Design of fluorescent materials for chemical sensing," *Chemical Society Reviews*, vol. 36, no. 6, pp. 993-1017, 2007.

[8] A. Shokry, M. M. A. Khalil, H. Ibrahim, M. Soliman, and S. Ebrahim, "Highly luminescent ternary nanocomposite of polyaniline, silver nanoparticles and graphene oxide quantum dots," *Scientific Reports*, vol. 9, no. 1, pp. 16984-16984, 2019.

[9] N. Orachorn, and O. Bunkoed, "A nanocomposite fluorescent probe of polyaniline, graphene oxide and quantum dots incorporated into highly selective polymer for lomefloxacin detection," *Talanta*, vol. 203, pp. 261-268, 2019.

[10] E. Pringsheim, D. Zimin, and O. S. Wolfbeis, "Fluorescent Beads Coated with Polyaniline: A Novel Nanomaterial for Optical Sensing of pH," *Advanced Materials*, vol. 13, no. 11, pp. 819-822, 2001.

[11] I. Z. Mohamad Ahad, S. Wadi Harun, S. N. Gan, and S. W. Phang, "Polyaniline (PAni) optical sensor in chloroform detection," *Sensors and Actuators B: Chemical*, vol. 261, pp. 97-105, 2018.

[12] C. M. Drain, J. T. Hupp, K. S. Suslick, M. R. Wasielewski, and X. Chen, "A perspective on four new porphyrin-based functional materials and devices," *Journal of Porphyrins and Phthalocyanines*, vol. 06, no. 04, pp. 243-258, 2002.

[13] Z.-L. Qi, Y.-H. Cheng, Z. Xu, and M.-L. Chen, "Recent advances in porphyrin-based materials for metal ions detection," *International Journal of Molecular* Sciences, vol. 21, no. 16, pp. 5839, 2020.

[14] M. Caselli, "Porphyrin-based electrostatically self-assembled multilayers as fluorescent probes for mercury(ii) ions: a study of the adsorption kinetics of metal ions on ultrathin films for sensing applications," *RSC Advances*, vol. 5, no. 2, pp. 1350-1358, 2015.

[15] S. Ajit, S. Palaniappan, P. U. Kumar, and P. Madhusudhanachary, "One-pot direct synthesis of fluorescent polyaniline-porphyrin macrospheres from porphyrin," *Journal of Polymer Science Part A: Polymer Chemistry*, vol. 50, no. 5, pp. 884-889, 2012.

[16] M. Khalid, J. J. S. Acuña, M. A. Tumelero, J. A. Fischer, V. C. Zoldan, and A. A. Pasa, "Sulfonated porphyrin doped polyaniline nanotubes and nanofibers: synthesis and characterization," *Journal of Materials Chemistry*, vol. 22, no. 22, pp. 11340-11346, 2012.

[17] R. K. Pandey, C. S. S. Sandeep, R. Philip, and V. Lakshminarayanan, "Enhanced optical nonlinearity of polyaniline-porphyrin nanocomposite," *The Journal of Physical Chemistry C*, vol. 113, no. 20, pp. 8630-8634, 2009.

[18] Y. Egawa, R. Hayashida, and J.-i. Anzai, "pH-induced interconversion between J-aggregates and H-aggregates of 5,10,15,20-tetrakis (4-sulfonatophenyl)porphyrin in polyelectrolyte multilayer films," *Langmuir*, vol. 23, no. 26, pp. 13146-13150, 2007.

[19] H. L. Ma, and W. J. Jin, "Studies on the effects of metal ions and counter anions on the aggregate behaviors of meso-tetrakis (p-sulfonatophenyl)porphyrin by absorption and fluorescence spectroscopy," *Spectrochimica Acta Part A: Molecular and Biomolecular Spectroscopy*, vol. 71, no. 1, pp. 153-160, 2008.

[20] M. M. Ayad, N. A. Salahuddin, M. O. Alghaysh, and R. M. Issa, "Phosphoric acid and pH sensors based on polyaniline films," *Current Applied Physics*, vol. 10, no. 1, pp. 235-240, 2010.

[21] L. Feng, Z. Chen, and D. Wang, "Selective sensing of Fe^{3+} based on fluorescence quenching by 2,6-bis(benzoxazolyl) pyridine with β-cyclodextrin in neutral aqueous solution," *Spectrochimica Acta Part A: Molecular and Biomolecular Spectroscopy*, vol. 66, no. 3. pp. 599-603, 2007.

[22] H. Jia, X. Gao, Y. Shi, N. Sayyadi, Z. Zhang*, Q. Zhao, Q. Meng, and R. Zhang, "Fluorescence detection of Fe^{3+} ions in aqueous solution and living cells based on a high selectivity and sensitivity chemosensor," *Spectrochimica Acta Part A: Molecular and Biomolecular Spectroscopy*, vol. 149, pp. 674-681, 2015.

[23] Q. Zhang, Y. Sun, M. Liu, and Y. Liu, "Selective detection of Fe^{3+} ions based on fluorescence MXene quantum dots via a mechanism integrating electron transfer and inner filter effect," *Nanoscale*, vol. 12, no. 3, pp. 1826-1832, 2020.

[24] J. Li, Q. Wang, Z. Guo, H. Ma, Y. Zhang, B. Wang, D. Bin, and Q. Wei, "Highly selective fluorescent chemosensor for detection of Fe(3+) based on Fe_3O_4@ZnO," (in eng), *Scientific Reports*, vol. 6, pp. 23558-23558, 2016.

[25] R. Kagit, M. Yildirim, O. Ozay, S. Yesilot, and H. Ozay, "Phosphazene based multicentered naked-eye fluorescent sensor with high selectivity for Fe^{3+} Ions," *Inorganic Chemistry*, vol. 53, no. 4, pp. 2144-2151, 2014.

[26] M. R. G. Fahmi, A. T. N. Fajar, N. Roslan, L. Yuliati, A. Fadlan, M. Santoso, and H. O. Lintang "Fluorescence study of 5-nitroisatin Schiff base immobilized on SBA-15 for sensing Fe^{3+}," *Open Chemistry*, vol. 17, no. 1, pp. 438-447, 2019.

[27] S. Tang, J. Sun, Y. Li, D. Xia, T. Qi, K. Liu, H. Deng, W. Shen, and H. K. Lee, "pH-dependent selective ion exchange based on (ethylenediamintetraacetic acid-nickel)-layered double hydroxide to catalyze the polymerization of aniline for detection of Cu^{2+} and Fe^{3+}," *Talanta*, vol. 187, pp. 287-294, 2018.

[28] Z. F. Gao, T. T. Li, X. L. Xu, Y. Y. Liu, H. Q. Luo, and N. B. Li, "Green light-emitting polyepinephrine-based fluorescent organic dots and its application in intracellular metal ions sensing," *Biosensors and Bioelectronics*, vol. 83, pp. 134-141, 2016.

[29] Y. R. Bhorge, H.-T. Tsai, K.-F. Huang, A. J. Pape, S. N. Janaki, and Y.-P. Yen, "A new pyrene-based Schiff-base: A selective colorimetric and fluorescent chemosensor for detection of Cu(II) and Fe(III)," *Spectrochimica Acta Part A: Molecular and Biomolecular Spectroscopy*, vol. 130, pp. 7-12, 2014.